RESEARCH ARTICLE | MARCH 28 2025

Minimizing read noise in liquid crystal x-ray detectors using particle-in-binder HgI_2 layers

Bong Gyu Rho ; Sam Hak Baek ; Young Suk An ; Wei Lei; Se Yong Choi ; Byung Seong Bae

Rev. Sci. Instrum. 96, 033103 (2025)
https://doi.org/10.1063/5.0231219

Review of Scientific Instruments ARTICLE pubs.aip.org/aip/rsi

Minimizing read noise in liquid crystal x-ray detectors using particle-in-binder HgI_2 layers

Cite as: Rev. Sci. Instrum. 96, 033103 (2025); doi: 10.1063/5.0231219
Submitted: 1 August 2024 • Accepted: 5 March 2025 •
Published Online: 28 March 2025

Bong Gyu Rho,[1] Sam Hak Baek,[1] Young Suk An,[1] Wei Lei,[2] Se Yong Choi,[3] and Byung Seong Bae[3,a)]

AFFILIATIONS

[1] Sesim Photonics Technology Co., Uiwang, Gyeonggi 16072, South Korea
[2] School of Electronic Science and Engineering, Southeast University, Nanjing 210000, China
[3] Department of the Semiconductor Engineering, Hoseo University, Asan, Chungnam 31499, South Korea

[a)] **Author to whom correspondence should be addressed:** bsbae3@hoseo.edu

ABSTRACT

A liquid crystal x-ray detector was manufactured by coating HgI_2 on a thin glass substrate liquid crystal cell in guest–host (GH) mode. The HgI_2 layer was produced using the particle-in-binder (PIB) method. A reflective optical system was constructed so that one pixel corresponds to a 45 × 45 μm^2 area of the liquid crystal cell. A quantification process was established to convert liquid crystal images into x-ray images. As a result, the signal-to-noise ratio (SNR) was 50 when irradiated with 32 keV, 10 mR/cm^2 x rays. In the liquid crystal x-ray detector, read noise decreases as the intensity of the light source increases. The full well capacity (FWC) of the image sensor was 100 ke, measured in the range of 25 ke to 70 ke, with a read noise of ~1%. To achieve an SNR at the shot noise level, an FWC of 500 ke is required, with measurements taken in the 100–400 ke range. In this case, the read noise is less than 0.3%, and the measurement precision approaches the physical limit.

I. INTRODUCTION

Reducing radiation exposure in x-ray imaging is crucial for safety, and achieving this requires a high signal-to-noise ratio (SNR) in the images. Enhancing SNR can be achieved by either increasing the output signal at a given radiation dose or by minimizing noise levels. The former involves research into photoconductors with high charge collection efficiency and scintillators that generate more photons.[1–3] The latter approach focuses on liquid crystal x-ray detectors, which can minimize read noise by increasing the intensity of the read beam and using a camera to capture the liquid crystal panel image.[4–6] This method eliminates the need for a TFT substrate and allows the entire image to be read using the camera, significantly reducing fixed pattern noise from data and gate lines. Furthermore, with a fill factor of 100%, the detection characteristics of liquid crystal x-ray detectors are similar to those of photon-counting x-ray detectors.[7–10]

Liquid crystal x-ray detectors measure the optical properties of light passing through a liquid crystal layer to determine the charge density in the photoconductive layer. The fundamental concept was introduced by Huignard *et al.* in 1983, involving a structure with a cholesteric liquid crystal layer on a photoconductive layer.[11] In 1998, the Rowland group presented the basic characteristics of a liquid crystal x-ray detector using reflective TN (Twist Nematic) mode and a line scan method.[12,13] Although the Rowland group developed a prototype for breast cancer detection, the further improvements were delayed due to challenges in quantifying liquid crystal images.[14] Another attempt was made by SESIM Photonic Technology, which developed a liquid crystal x-ray detector using a transmissive optical system and amorphous Se.[15,16] However, issues with DC disturbance in the liquid crystal layer and charge removal trapped in the bandgap of the Se led to a halt in further development. Meanwhile, the rise of direct and indirect DR (Digital Radiography) based on TFT (thin-film transistor) array technology being used in FPD (Flat Panel Display) diminished the use of liquid crystal x-ray detectors.[17–19]

Liquid crystal x-ray detectors offer several advantages. By optimizing the intensity of the read beam, the thickness of the liquid crystal layer, and the design parameters of the liquid crystal, sensitivity can be maximized. In addition, the liquid crystal layer can

be measured multiple times as long as it maintains its voltage.[16] In particular, increasing the intensity or duration of the read beam and using cameras with high Full Well Capacity (FWC) can drastically reduce read noise. Furthermore, the production process for liquid crystal panels and the assembly of optical systems, including cameras, are relatively simple and cost-effective compared to TFT array-based DR systems. Mercuric iodide (HgI_2) was used in this liquid crystal x-ray detector. HgI_2, extensively studied for detector applications, was adopted as a photoconductor due to its superior stability to other materials such as selenium (Se). While Se undergoes crystallization and structural changes over time, HgI_2 maintains its structural and electrical integrity under prolonged operation. Its wide bandgap (~2.1 eV) enables low dark current operation, reducing noise and enhancing signal quality. In addition, HgI_2 exhibits high x-ray absorption efficiency due to its high atomic number (Hg: 80, I: 53), making it particularly suitable for direct-conversion x-ray and gamma-ray detectors. Furthermore, its relatively high electron mobility (~10 cm^2/V s) compared to Se (~0.2 cm^2/V s) contributes to efficient charge transport and collection, improving detector sensitivity and spatial resolution. Therefore, HgI_2 was adopted as a photoconductive material in liquid crystal detectors, where its high detection signal, supported by an optimized drive scheme, enables effective noise reduction and improved imaging performance.

II. EXPERIMENTAL

The structure of the liquid crystal x-ray detector and the process used in this study are illustrated in Figs. 1(a) and 1(b), respectively. The detector consists of a GH (Guest Host) liquid crystal cell on a thin glass substrate, which is coated with a photoconductor layer of HgI_2. GH liquid crystal cell is formed between a glass coated with ITO and a bare glass without ITO electrode. The glass substrate without ITO electrode is lapped and polished to a thickness of ~50 μm.

The HgI_2 layer, deposited using the particle in binder (PIB) method, has a thickness of ~200 μm. HgI_2 was initially acquired in powdered form and subsequently processed through ball milling to achieve a fine and uniform particle distribution suitable for the PIB application. For ball milling, HgI_2, polyvinyl butyral (PVB), and butyl cellosolve were mixed in a weight ratio of 20:1:4, respectively. The resulting slurry was further processed using a three-roll mill to refine particle dispersion and enhance uniformity, followed by thorough mixing in a planetary mixer to ensure homogeneity.

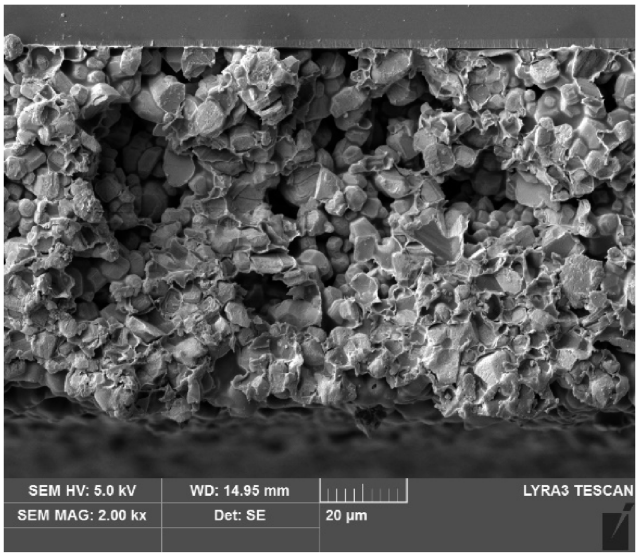

FIG. 2. Scanning electron microscope (SEM) image of the binder-integrated film.

After mixing, the slurry was subjected to a controlled drying process at 65 °C for 72 h,[20,21] allowing solvent evaporation and proper binder integration. The dried HgI_2 composite was then bonded onto an ITO-coated glass substrate using a UV-curing adhesive (3052; ThreeBond) to achieve strong adhesion and electrical contact. These processing steps were optimized to maintain the structural integrity of HgI_2 while ensuring uniform layer formation, critical for stable photoconductive performance in detector applications. Figure 2 shows the scanning electron microscope (SEM) image of the binder-integrated film.

The thickness of the HgI_2 (mercury iodide) layer in mammography applications is typically set between 150 and 200 μm to balance optimal x-ray absorption with image clarity. This thickness range

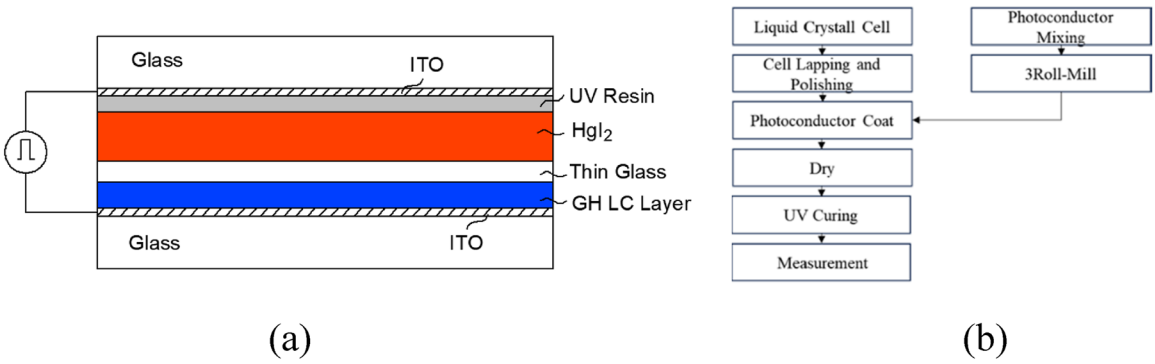

FIG. 1. Structure of the liquid crystal x-ray detector used in this study (a) and the fabrication process (b).

ensures that enough x rays are absorbed to generate a strong signal without causing excessive blur or loss of spatial resolution. A thicker layer would absorb more x rays but could lead to image degradation due to scattered charge carriers, while a thinner layer would reduce signal strength. In addition, this thickness allows for efficient charge collection, improving signal-to-noise ratio and overall image quality, which is essential for clear mammographic images. Finally, the 150–200 μm thickness is also feasible from a manufacturing standpoint, ensuring uniformity and mechanical stability in large-area detectors.

While the thin glass substrate can interfere with resolution by spreading the electric field, removing it would require a protective layer between the photoconductor and the liquid crystal layer to prevent contamination. This necessitates very precise equipment and processes. However, using a thin glass substrate simplifies the independent processing of the liquid crystal and photoconductor layers, facilitating easy and quick evaluation of photoconductor properties and measurement standards.

Figure 3(a) shows the waveform and synchronization signals applied to the liquid crystal panel. When a separation voltage (Vs) is applied and the detector is exposed to x rays, electrons and holes generated in the photoconductor move in opposite directions. Holes accumulate on the thin glass substrate of the liquid crystal layer, while electrons gather beneath the UV-curing adhesive.[7,13] The accumulated hole charge creates an electric field within the liquid crystal layer, effectively modulating the transmitted polarized light. As the accumulated charge varies with the intensity of incident x rays, this modulated light forms the image on the x-ray detector, subsequently captured using a camera to measure the charge amount.

The polarity of the applied voltage determines whether the charge is accumulated by holes or electrons on the thin glass of the liquid crystal layer. While the total extracted charge amounts are comparable regardless of polarity, holes exhibit superior resolution characteristics due to their quicker removal of trapped charges. The separation voltage was 1 V per micrometer of thickness of HgI_2. The measurement voltage (Vm) was set above the liquid crystal's threshold voltage during x-ray imaging. Electrons in HgI_2 are more susceptible to trapping than holes, primarily due to the presence of deeper trap states that attract electrons more strongly. These trap states, often linked to defects such as vacancies or impurities in the crystal lattice, increase the likelihood of electron trapping, which can result in recombination and charge loss if the trapped electrons are not efficiently removed by the applied electric field.

In contrast, holes are less susceptible to trapping in HgI_2. The material's electronic structure favors the transport of holes over long distances with fewer interruptions, allowing for faster and more efficient charge collection. Holes also exhibit a lower tendency to recombine with electrons after separation, further facilitating efficient charge extraction. The trap energy levels in HgI_2 are generally more conducive to trapping electrons, making it more challenging for electrons to escape once trapped. As a result, holes contribute to better resolution in imaging systems by clearing trapped charges more quickly, improving the signal-to-noise ratio and image clarity. While electrons have higher mobility, their higher susceptibility to trapping requires higher electric field strength or longer collection times to achieve optimal charge extraction. Holes, with their faster charge collection and reduced recombination, provide superior resolution, making them more beneficial for high-resolution imaging applications in HgI_2-based detectors.

For HgI_2, an electric field strength of ~1 V/μm is sufficient to achieve efficient charge transport and collection without causing excessive leakage current or breakdown of the material. This voltage ensures that both electrons and holes can be effectively driven toward their respective electrodes, optimizing the signal extraction process. It also minimizes the risk of trapping and recombination, which could degrade the performance of the detector. By selecting this field strength, a balance between efficiency and stability is achieved, ensuring optimal operation of the detector without requiring unnecessarily high voltages that could compromise the material's integrity.

The optical system can be classified into transmissive and reflective types based on whether the read beam passes through or is reflected by the photoconductor. Figure 3(b) depicts the reflective optical system used in this study. Reflective systems offer greater flexibility in the positioning of the light source compared to transmissive systems. As shown in Fig. 3(b), two light sources were used, and the camera module was set to capture the reflected light image. The TN-1239 liquid crystal was doped with 3% anisotropic dye AC4 (NEMATEL) by weight. The liquid crystal cell was aligned in parallel, with the rubbing direction parallel to the analyzer's transmission axis.

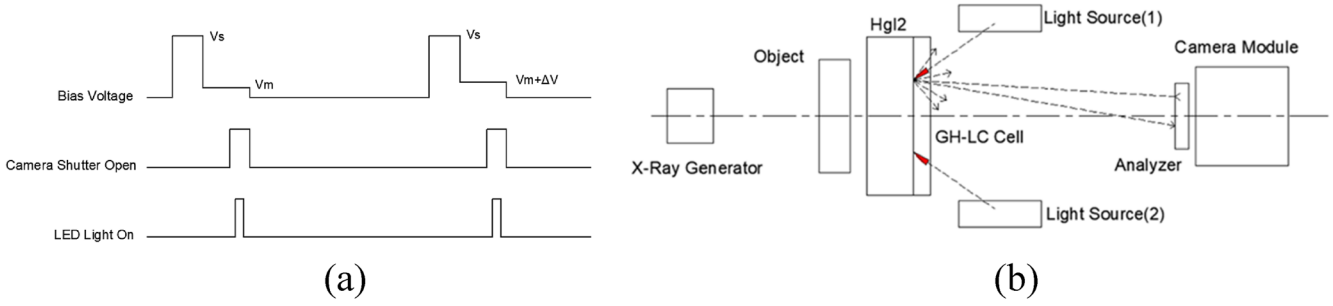

FIG. 3. Timing diagram for imaging the incident x ray (a) and reflective optical system used in this study (b).

III. RESULTS AND DISCUSSION

Figure 4(a) shows the transmission spectrum of PIB HgI_2, which has a bandgap of ~2.13 eV, corresponding to a wavelength of around 580 nm. Therefore, the read beam must have a wavelength longer than 580 nm to avoid absorption by the HgI_2 layer, which would generate electron–hole pairs and charge up the HgI_2 layer.

In addition, the beam must be well absorbed by the anisotropic dye. A 660nm LED was used as the light source. Light from the LED passes through the liquid crystal cell, is diffusely reflected by the PIB HgI_2 layer, and then passes back through the liquid crystal cell. The light is selectively transmitted using the analyzer into the camera to capture the x-ray image.

The primary difference between liquid crystal x-ray detectors and DDR (Direct Digital Radiography) systems lies in the need for an external current-to-voltage conversion process in DDR systems, which is absent in liquid crystal x-ray detectors.[22–24] In DDR systems, charges generated by x-ray excitation in the photoconductor are stored in a pixel's storage capacitor to control the gate voltage of the transistor. These gate voltages regulate the currents through the transistor, which are then converted to voltages using an external charge–voltage conversion circuit after flowing to the outer circuit. In contrast, liquid crystal x-ray detectors detect voltage changes in the liquid crystal layer by directly collecting charges on the thin glass substrate within the layer, bypassing the need for current transfer to an external circuit. This direct charge collection mechanism enhances the efficiency of the detection process, as it minimizes energy losses associated with the external circuitry. By utilizing the glass substrate as an integral part of the detection system, the liquid crystal layer can respond more rapidly to x-ray exposure, allowing for more precise and real-time imaging. In addition, this approach reduces the complexity of the detector design, as it eliminates the need for intricate charge readout systems typically required in conventional x-ray detectors. Furthermore, the direct charge accumulation on the substrate allows for improved spatial resolution and faster response times, as the charges are captured locally without the delays inherent in transferring signals through external circuits. This configuration is particularly advantageous for applications requiring high-speed imaging and real-time analysis, such as in medical diagnostics and security screening. Since the liquid crystal imaging can determine the distribution of trapped charges in the photoconductor material before x-ray exposure, it can compensate for the effect of the residual trap charge.

TABLE I. Specification of the camera used in this study.

Item	Specification
Manufacturer (model)	FLIR(BFS-U3-17S7M-C)
Resolution	1600 × 1100
Sensor (CMOS)	Sony IMX425
Pixel pitch	9 μm
Full well capacity (saturation)	98 654 e–
Dark noise	22.99 e–

In x-ray detectors, image quality is affected by read noise (electron noise) at low exposure levels and by shot noise and fixed pattern noise at higher exposure levels. The absolute amount of noise is given by the following equation:

$$\sigma \propto \left[\sigma(Read)^2 + \sigma(Shot)^2 + \sigma(Fixed\ Pattern)^2\right]^{0.5}. \quad (1)$$

Liquid crystal x-ray detectors can significantly reduce read noise by increasing the intensity of the light passing through the liquid crystal layer. The brightness of the light source is determined by the Full Well Capacity (FWC) of the camera. Table I lists the main specifications of the camera used in this study.

When the dynamic range of the liquid crystal image is set between 20 and 60 ke, including a dark noise of 22.9 e, the read noise of the camera can be calculated using the following equation:

$$\sigma\_camera(Read) \propto \left[\sigma\_camera(Shot)^2 + \sigma\_camera(Dark\ noise)^2\right]^{0.5}. \quad (2)$$

In this optical system, the read noise of the liquid crystal ranges from 0.41% to 0.71%. If the FWC is 500 ke and the dynamic range of the liquid crystal image is set between 100 ke and 400 ke, the read noise can be limited to between 0.16% and 0.32%.

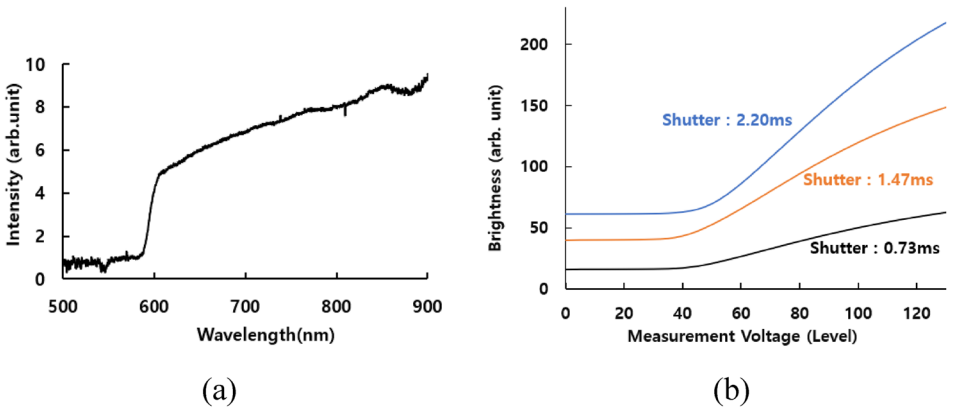

FIG. 4. Transmission spectrum of the PIB HgI_2 (a) and voltage–reflectance curve obtained without the application of incident x ray (b).

The liquid crystal image is somewhat correlated with the charge quantity excited in the photoconductor, but an exact relationship must be established. The reference reflectance curve is obtained by applying a separation voltage (Vs) consistently to the liquid crystal panel while varying the measurement voltage (Vm) without x-ray exposure. This reference reflectance curve is synchronized with the camera shutter and LED light source. The brightness of the light source is adjusted by the camera shutter's opening time, which should be longer than the light source's on–off cycle for higher measurement accuracy. Figure 4(b) presents an example of the voltage–reflectance curves obtained without the application of incident x rays. The curve reflects the residual charge in the photoconductor layer. The liquid crystal image obtained under x rays is compared to the reference reflectance curve to determine the corresponding value for the actual x-ray image. First, the voltage on the reference voltage–reflectance curve that matches the brightness of the x-ray image is determined. Subtracting the reference measurement value from the determined value under x rays yields a value proportional to the charge induced by the incident x rays.[16] For accurate measurement, sufficient removal time is necessary to eliminate the effect of trap charge caused by the read beam.

During x-ray exposure, a separation voltage (Vs) is applied to separate electrons and holes. The voltage is then changed to the measurement voltage, which is higher than the liquid crystal's threshold voltage. After a short period, the reflectance is measured. The separation voltage for the photoconductor is approximately 1 V per micrometer of thickness. If the applied voltages corresponding to the same reflectance on the reference curve are denoted as V(r), then the charge density (σ) induced by the x rays is given by the following equation:

$$\sigma = C(ph) \cdot (V(r) - V(m)). \tag{3}$$

C(ph) is the capacitance of the photoconductor. By knowing the reference reflectance curve and the reflectance of the pixel measured with the applied voltage after x-ray exposure, the x-ray charge amount can be directly determined from Eq. (3).

The trap charges in the photoconductor during measurements distort the voltage signal and therefore need correction. The reference reflectance curve is measured without any accumulated charge. The trapped charge inside the HgI_2 can be determined by applying a signal, as shown in Fig. 3(a), and comparing it to the reference reflectance curve. In addition, the uniformity of the x-ray source

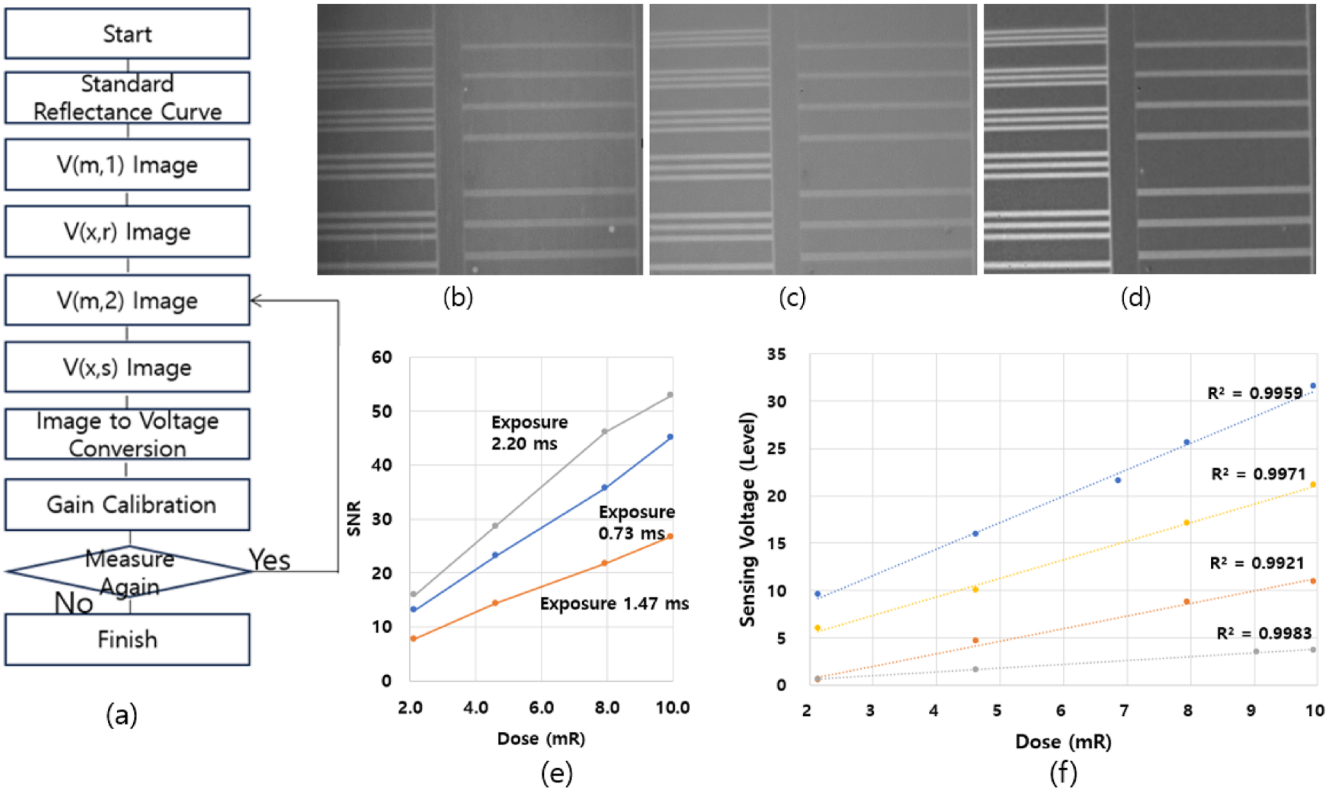

FIG. 5. Measurement procedure of the developed x-ray detector (a), the x-ray image (b), the interpolated voltage image obtained using the reference reflectance curve (c), the line phantom image after gain calibration (d), SNR variation with different illumination intensities of the read beam relative to the exposure dose (e), and the linearity of the liquid crystal x-ray detector (f).

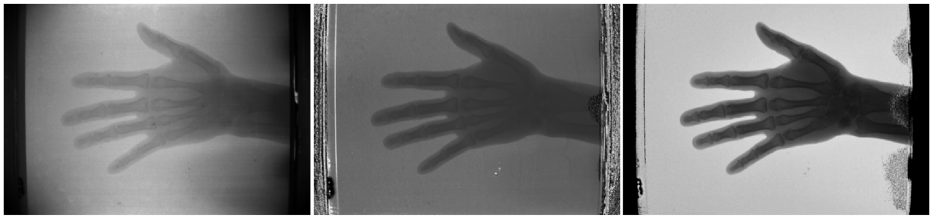

FIG. 6. (a) Measurement screen, (b) voltage image, and (c) gain-calibrated screen.

distribution needs to be corrected. In the following equation, V(x,s) represents the measured signal when the x ray irradiates the object and V(x,r) represents the signal when the x ray irradiates without any object. V(m,1) and V(m,2) are signals measured by applying only the measurement voltage (Vm) before x-ray irradiation. Gain calibration is performed as follows:

$$X = \frac{V(x,s) - V(m,1)}{V(x,r) - V(m,2)}. \quad (4)$$

The x-ray generator used in this experiment was an AJEX 200H from AJEX Meditech. A camera lens from SIWON Optical Technology was used to ensure that each pixel corresponded to a 45 ×45 μm^2 area of the liquid crystal cell. The light source was a 660 nm LED array arranged bi-directionally to enhance luminance uniformity. The tube voltage of the x-ray generator was fixed at 80 kV. The distance between the liquid crystal panel and the x-ray generator was 1.8 m. The exposure dose and HVL (Half-Value Layer) were measured using a RaySafe X2, from which the effective energy was determined. The camera, driving waveforms, and light source were controlled via an Arduino module connected to a PC.

Figure 5(a) illustrates the measurement procedure. Care was taken to prevent DC voltage accumulation in the liquid crystal during the measurement of the reference reflectance curve. After applying the measurement waveform, images were captured only after the liquid crystal response had stabilized. The liquid crystal images were converted using interpolation based on the reference reflectance curve voltage and gain calibration. Since trap charges vary momentarily, V(m,1) and V(m,2) images were measured before x-ray exposure for correction. To reduce the influence of shot noise, the x-ray exposure was repeated eight times, and the average was used to establish the reference x-ray image. Both the reference reflectance curve and the reference x-ray image could be reused as long as the measurement conditions remained constant. For gain calibration, images were taken without x-ray exposure [V(m,1)] and reference x-ray images without the object [V(x,r)]. Subsequently, x-ray sample images were captured, followed by images without x-ray exposure [V(m,2)] and sample images [V(x,s)].

Figure 5(b) presents the x-ray image, the interpolated voltage image obtained using the reference reflectance curve (c) and the line phantom image after gain calibration (d). It is evident that the images become more refined at each transformation stage from the liquid crystal image to the voltage image and finally to the gain-calibrated image. The line phantom was distinguishable up to 4.6-line pairs per millimeter (ls/mm). To measure SNR, the sample images were acquired at 80 kVp and 4 mA s with an exposure dose of 10 mR. The reference x-ray image was averaged from eight measurements at 12.5 mR. The x-ray generator's HVL was 3.2 mm Al, resulting in an effective energy of ~32 keV. Using "ImageJ" for analysis, the gain-calibrated image showed an SNR of 54 over a 100 × 100 pixel area. Given that each pixel (45 × 45 μm^2) received about 5670 photons at 10 mR/cm^2 for a 50 kVp x ray, the theoretical SNR due to shot noise is 75. For 20 keV, the photon count per pixel is 1,113, yielding a theoretical SNR of 33 due to shot noise.[12,13] Although there are no specific data for photon density at 32 keV, the results indicate minimal impact from read noise.

Figure 5(e) shows the SNR variation with different illumination intensities of the read beam relative to the exposure dose. As the illumination intensity increases, the SNR also increases, demonstrating the effect of enhanced light intensity. Figure 5(f) illustrates the linearity of the liquid crystal x-ray detector. Despite some variation between samples, the linearity (R) ranged from 0.9928 to 0.9983. The range of x-ray exposure can be extended by adjusting the separation voltage.

Figures 6(a)–6(c) display measurement images of a hand on a 30 × 24 cm^2 screen. The liquid crystal screen was processed using ultra-thin glass. Image (a) shows the measurement screen, (b) is the voltage image, and (c) is the gain-calibrated screen. The size of the display can be increased if the liquid crystal panel is fabricated larger.

IV. CONCLUSION

By combining a liquid crystal cell in GH mode with HgI_2, we developed a reflective x-ray liquid crystal detection system and established a method to determine x-ray dosage quantitatively. It was shown that as light intensity increases, read noise decreases, thereby increasing the SNR. A process was established to detect charges trapped in the bandgap and minimize their impact. When the FWC is 1 Me, setting the measurement range between 100 ke and 600 ke can reduce read noise to below 0.35%. The liquid crystal x-ray detector has a simple fabrication process, low material costs, and can reduce radiation exposure, making it highly viable for commercialization. It is particularly promising for mammography applications.

ACKNOWLEDGMENTS

We express our gratitude to Professor Seung-Eon Ahn from the Department of Nano-Optical Engineering at Korea Polytechnic

University for his valuable advice on HgI_2. This work was supported by the National Research Foundation of Korea grant funded by the Korean Government (Grant No. NRF- 2022K1A3A1A20015124).

AUTHOR DECLARATIONS

Conflict of Interest

The authors have no conflicts to disclose.

Author Contributions

Bong Gyu Rho: Writing – original draft (equal). **Sam Hak Baek**: Software (equal). **Young Suk An**: Formal analysis (equal); Methodology (equal). **Wei Lei**: Conceptualization (equal). **Se Yong Choi**: Data curation (equal). **Byung Seong Bae**: Writing – review & editing (equal).

DATA AVAILABILITY

The data that support the findings of this study are available from the corresponding author upon reasonable request.

REFERENCES

[1]P. Jin, Y. Tang, D. Li, Y. Wang, P. Ran, C. Zhou, Y. Yuan, W. Zhu, T. Liu, K. Liang, C. Kuang, X. Liu, B. Zhu, and Y. Yang, "Realizing nearly-zero dark current and ultrahigh signal-to-noise ratio perovskite X-ray detector and image array by dark-current-shunting strategy," Nat. Commun. **14**, 626 (2023).
[2]L.-J. Xu, X. Lin, Q. He, M. Worku, and B. Ma, "Highly efficient eco-friendly X-ray scintillators based on an organic manganese halide," Nat. Commun. **11**, 4329 (2020).
[3]Y. Song, S. Wang, X. Zhao, Q. Hu, C. Huang, G. Meng, V. Gnatyuk, Y. Ni, and H. Wu, "Significant sensitivity enhancement of single crystal CdSe x-ray detector by liquid nitrogen cooling," Appl. Phys. Lett. **123**, 032102 (2023).
[4]S. Hejazi and D. P. Trauernicht, "System considerations in CCD-based x-ray imaging for digital chest radiography and digital mammography," Med. Phys. **24**, 287 (1997).
[5]J. Grinberg, A. Jacobson, W. Bleha *et al.*, "A New real-time non-coherent to coherent light image converter the hybrid field effect liquid crystal light valve," Opt. Eng. **14**, 217 (1975).
[6]D. Armitage, J. I. Thackara, W. D. Eades, L. Miller, L. Fraas, D. Boswell, and G. Myer, "Photoaddressed liquid crystal spatial light modulators," Appl. Opt. **28**, 4763 (1989).
[7]B. Kreisler, "Photon counting detectors: Concept, technical challenges, and clinical outlook," Eur. J. Radiol. **149**, 110229 (2022).
[8]C. H. McCollough, K. Rajendran, S. Leng, L. Yu, J. G. Fletcher, K. Stierstorfer, and T. G. Flohr, "The technical development of photon-counting detector CT," Eur. Radiol. **33**, 5321 (2023).
[9]S. Aubert and J. Tanguay, "Experimental optimization of single-exposure dual-energy angiography with photon-counting x-ray detectors," Med. Phys. **50**, 763 (2023).
[10]Y. Zhou, C. Fei, M. A. Uddin, L. Zhao, Z. Ni, and J. Huang, "Self-powered perovskite photon-counting detectors," Nature **616**, 712 (2023).
[11]J. P. Huignard, S. Berre, C. Mayeux, and F. Micheron, "Liquid crystal image converter," U.S. patent 4,368,386 (11 January 1983).
[12]P.-K. Rieppo and J. A. Rowlands, "X-Ray imaging with amorphous selenium: Theoretical feasibility of the liquid crystal light valve for radiography," Med. Phys. **24**(8), 1279 (1997).
[13]T.-C. Szeto, C. A. Webster, I. Koprinarov, and J. A. Rowlands, "The x-ray light valve: A potentially low-cost, digital radiographic imaging system—A liquid crystal cell design for chest radiography," Med. Phys. **35**(3), 959 (2008).
[14]S. Marcovici, V. Sukhovatkin, and P. Oakham, "X-ray light valve (XLV): A novel detectors' technology for digital mammography," SPIE Proc. **9033**, 90333N-1–90333N-6 (2014).
[15]B. G. Rho, "A new X-ray image sensor utilizing a liquid crystal panel," Hankook Kwanghak Hoeji **19**(4), 249 (2008).
[16]B. G. Rho, S. H. Baek, S. J. Kang, J. M. Lee, and B. S. Bae, "Development of X-ray detector using liquid crystal with front light," J. Korean Soc. Radiol. **13**, 831 (2019).
[17]A. R. Cowen, S. M. Kengyelics, and A. G. Davies, "Solid-state, flat-panel, digital radiography detectors and their physical imaging characteristics," Clin. Radiol. **63**, 487 (2008).
[18]T. Zou, B. Xiang, Y. Xu, Y. Wang, C. Liu, J. Chen, K. Wang, Q. Dai, S. Zhang, Y.-Y. Noh, and H. Zhou, "Pixellated perovskite photodiode on IGZO thin film transistor backplane for low dose Indirect X-ray detection," IEEE J. Electron Devices Soc. **9**, 96 (2021).
[19]C. R. Newman, H. Sirringhaus, J. C. Blakesley, and R. Speller, "Stability of polymeric thin film transistors for x-ray imaging applications," Appl. Phys. Lett. **91**, 142105 (2007).
[20]J. C. Park and S.-E. Ahn, "Dynamic properties of flat-panel X-ray image sensors with mercury iodide photoconductors undergoing repeated X-ray irradiation," IEEE J. Electron Devices Soc. **5**(5), 400 (2017).
[21]D. Lee, K. Lee, and J. Seo, "High signal-to-noise ratio HgI_2 X-ray detector assisted with ultraviolet radiation," Nucl. Instrum. Methods Phys. Res., Sect. A **941**, 162364 (2019).
[22]A. Levi, M. M. Schieber, and Z. Burshtein, "Dark current transients in HgI_2 single crystals used as γ- and x-ray spectrometers," J. Appl. Phys. **57**, 1944 (1985).
[23]A. C. Konstantinidis, "Evaluation of digital X-Ray detectors for medical image applications," Ph.D. thesis, University College London, 2010.
[24]J. A. Seibert, "Flat-panel detectors: How much better are they?," Pediatr. Radiol. **36**, 173 (2006).